Supplementary Information for

Facile activation of an unconjugated zwitterionic squaraine dye for tunable fluorescence and morphology behaviors

Weihan Guo [ab], Yinhe Qu [e], Mingda Wang [ab], Guomin Xia [abd*], Hongming Wang [abc*]

[a] Institute for Advanced Study, Nanchang University, Nanchang 330031, China.

[b] Jiangxi Provincial Key Laboratory of Functional Crystalline Materials Chemistry, Nanchang 330031, China.

[c] College of Chemistry and Chemical Engineering, Nanchang University, Nanchang 330031, China.

[d] Department of Ecology and Environment, Yuzhang Normal University, Nanchang 330103, China.

[e] Key Laboratory of Green Chemistry & Technology, Ministry of Education, College of Chemistry, Sichuan University, Chengdu 610064, China.

[*] Email: hongmingwang@ncu.edu.cn, guominxia@ncu.edu.cn

Table of Content

Materials and instruments 1

Synthesis 2

Photophysical data in solution 3

Preparations of microcrystals 3

Photophysical data in crystal 4

Computational study 5

Preparations and characterizations of single crystals 6

Crystal structure analysis 10

Characterizations of vapoluminescence behavior 16

^{1}H NMR, ^{13}C NMR and MS spectra 17

Reference 20

Materials and instruments

All chemicals and solvents were purchased from commercial suppliers and used as received unless explicitly stated. Using TMS as an internal standard, ^{1}H NMR and ^{13}C NMR spectra were measured on a Bruker AVANCE 400 spectrometer in DMSO-d_6. UV-visible absorption spectra were recorded on a Lambda 750 spectrophotometer. Photoluminescence (PL) spectra were recorded on a Horiba FluoroMax-4 luminescence spectrometer. The absolute PL quantum efficiencies (Φ_{PL}) were determined using a Horiba FL-3018 Integrating Sphere. The fluorescence lifetime measurement was performed on a Horiba FluoreCube spectrofluorometer system using a UV diode laser (NanoLED 360 nm) for excitation. Scanning electron microscopy (SEM) images were collected on a Hitachi S-4300 instrument. Mass spectra were obtained with Trip TOFTM 5600 mass spectrometers. Thermogravimetric analysis (TGA) was carried out on a TG instrument (PerkinElmer STA 6000, USA) at a heating rate of 20 °C min^{-1} under an N_2 atmosphere. Powder X-ray diffraction (PXRD) data were collected using an XD-2 Purkinje multi-crystal X-ray diffractometer in parallel beam geometry employing CuKα radiation at 40 kV and 30 mA. The diffraction data were collected in the 2θ range from 5° to 30° at the scanning speed of 1.54 seconds per step with 2θ step increment of 0.01°. The X-ray diffraction experiments were carried out on a Bruker SMART APEX-II Single-crystal diffractometer at room temperature. All the structures were resolved and analyzed with the assistance of Olex2 software.

Synthesis

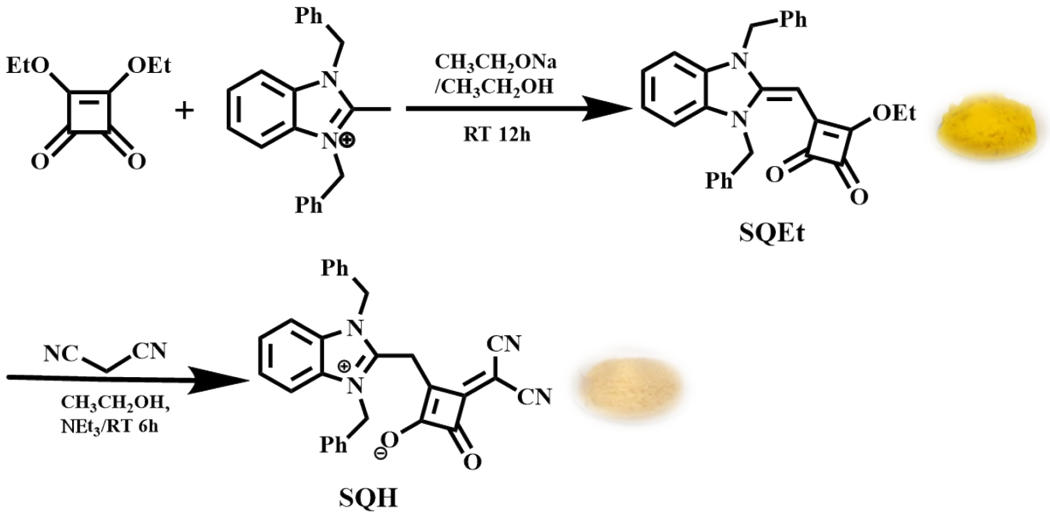

Scheme S1 The synthetic route of the unexpected unconjugated zwitterionic SQH (inset: corresponding photographs of SQEt and SQH).

Synthesis of SQEt:

Benzimidazolium salts were synthesized by our reported literature[1]. In a 100ml round bottomed flask, Na (0.11 g, 5 mmol) was dissolved in 50ml ethanol, after this diethyl squarate (0.85 g, 5 mmol) and 1,3-dibenzyl-2-methyl-benzimidazolium chloride (0.698 g, 2 mmol) were added successively. The mixture was stirred at 25 ℃ for 12 h under nitrogen, the resulting precipitate was filtered off and washed with ethanol to give crude product. The crude product was then purified via column chromatography (dichloromethane/methanol = 100 : 1) to yield yellow powder SQEt (1.37 mmol, 0.6 g, 69%). ^{1}H NMR (400 MHz, DMSO-d_6) δ: 7.57 (dd, J = 5.9, 3.2 Hz, 2H), 7.31 (t, J = 7.3 Hz, 4H), 7.27 (d, J = 3.0 Hz, 2H), 7.25 (d, J = 2.3 Hz, 2H), 7.12 (d, J = 7.3 Hz, 4H), 5.57 (s, 4H), 4.84 (s, 1H), 4.65 (q, J = 7.0 Hz, 2H), 1.35 (t, J = 7.0 Hz, 3H) ppm; ^{13}C NMR (100 MHz, DMSO-d_6) δ: 194.19, 179.59, 168.94, 151.72, 135.50 132.11, 128.77, 127.81, 126.73, 123.98, 111.23, 68.16, 63.18, 47.84, 15.67 ppm; HRMS (ESI) m/z: $[M + H]^+$ calcd, 437.1787; found, 437.1850.

Synthesis of SQH:

To ethanol (15 mL) was added SQEt (1.0 mmol, 437 mg), malononitrile (2.0 mmol, 202 mg) and triethylamine (2.0 mmol, 202 mg) in the 50 ml round bottomed flask. The mixture was stirred at 25 ℃ for 6 h under nitrogen, the resulting precipitate was filtered off and washed with ethanol to give crude orange powder. The resultant powder was purified via column chromatography (dichloromethane/methanol = 40:1) to give a colorless product SQH (0.83 mmol, 380 mg, 83%). ^{1}H NMR (400 MHz, DMSO-d_6) δ: 7.95-7.92 (m, 2H), 7.66-7.63 (m, 2H), 7.35-7.27 (m, 10H), 5.87 (s, 4H), 4.81 (s, 2H) ppm; ^{13}C NMR (100 MHz, DMSO-d_6) δ: 194.82, 187.53, 182.61, 161.12, 150.68, 134.32, 131.66, 129.16, 128.75, 127.62, 127.33, 117.91, 116.38, 114.16, 49.23, 22.38 ppm; HRMS (ESI) m/z: $[M + H]^+$ calcd, 457.1586; found, 457.1648.

Photophysical data in solution

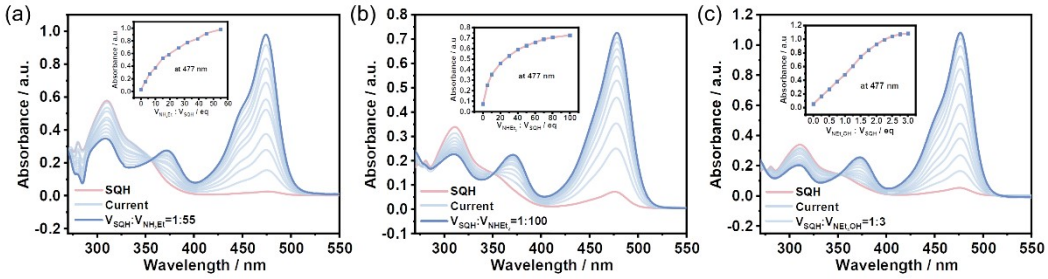

Fig. S1 Absorption spectral changes of SQH (50 μM) in THF upon the gradual addition of NH_2Et, $NHEt_2$, or NEt_4OH (inset: plots of absorbance at 477nm with different equivalents of amines).

Preparations of microcrystals

The SQH microcrystals were obtained in dichloromethane/methanol eluent during the column chromatography process.

All the ionic microcrystals (SQ-NH_3Et, SQ-NH_2Et_2, SQ-$NHEt_3$, and SQ-NEt_4) were prepared via a liquid phase self-assembly method.

(1) For SQ-NH_3Et microcrystals, 50 mg SQH was utterly dissolved in the 4 mL dichloromethane solution of ethylamine (2 M), after that 1 mL n-hexane was added

followed by vigorous sonication for 5 min. After cooling and aging in closed tubes at room temperature for 30 min, the corresponding assemblies with suitable dimensions were formed in the solutions.

(2) For SQ-NH_2Et_2 and SQ-$NHEt_3$ microcrystals, 50 mg SQH was completely dissolved in 4 mL dichloromethane/amine (volume ratio is 1:1) solution with vigorous sonication for 5 min. After cooling and aging in closed tubes at room temperature for 30 min, the corresponding assemblies with suitable dimensions were formed in the solutions.

(3) For SQ-NEt_4 microcrystals, 50 mg SQH was completely dissolved in 7 mL dichloromethane/n-hexane/dried NEt_4OH (volume ratio is 1:4:2) solution with vigorous sonication for 10 min. After cooling and aging in closed tubes at room temperature for 60 min, the corresponding assemblies with suitable dimensions were formed in the solutions.

All these ionic microcrystals were then used to prepare samples for further characterization.

Photophysical data in crystal

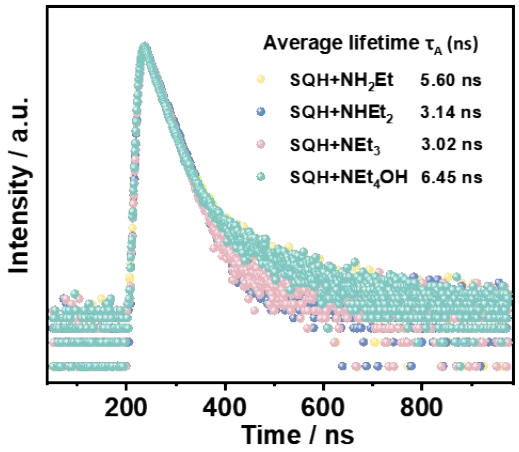

Fig. S2 Time-resolved fluorescence lifetimes of SQH (50 μM) at liquid nitrogen (77 K) in THF with the addition of different amines.

Table S1 The photophysical data for SQH (50 μM) at liquid nitrogen (77 K) in THF with the addition of different amines.

Addition	λ_{em} [a] [nm]	Φ_{PL} [b] %	Lifetime τ_f [c] [ns]	χ^2	k_f [d] [10^7 s^{-1}]	k_{nr} [e] [10^7 s^{-1}]
NH_2Et	490	63.4	5.60	1.01	11.32	6.54
$NHEt_2$	489	72.9	3.14	1.02	23.22	8.63
NEt_3	492	82.5	3.02	1.03	27.32	5.79
NEt_4OH	489	59.7	6.45	1.07	9.26	6.25

[a] Measured using an integrating sphere method; [b] Measured using a double-photocounting method; [c] Radiative rate constant ($k_f = \Phi_{PL} / \tau_f$); [d] Nonradiative rate constant ($k_{nr} = (1-\Phi_{PL}) / \tau_f$).

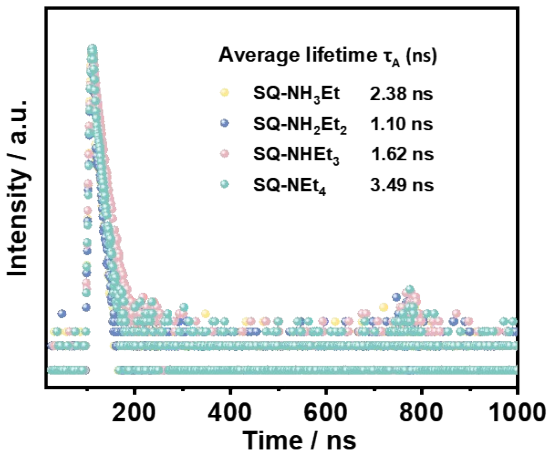

Fig. S3 (a) Fluorescence quantum yields (Φ_{PL}) and (b) time-resolved fluorescence lifetimes of SQ-NH_3Et, SQ-NH_2Et_2, SQ-$NHEt_3$, and SQ-NEt_4 ionic microcrystals at room temperature.

Table S2 The photophysical data for SQ-NH_3Et, SQ-NH_2Et_2, SQ-$NHEt_3$, and SQ-NEt_4 microcrystals.

Microcrystals	λ_{em} [a] [nm]	Φ_{PL} [b] %	Lifetime τ_f [c] [ns]	χ^2	k_f [d] [10^7 s^{-1}]	k_{nr} [e] [10^7 s^{-1}]
SQ-NH_3Et	533	27.3	2.38	1.01	11.47	30.55
SQ-NH_2Et_2	533	68.2	1.10	1.03	62.00	28.90
SQ-$NHEt_3$	532	57.7	1.62	1.00	35.62	26.11
SQ-NEt_4	531	18.6	3.49	1.04	5.33	23.32

[a] Measured using an integrating sphere method; [b] Measured using a double-photocounting method; [c] Radiative rate constant ($k_f = \Phi_{PL} / \tau_f$); [d] Nonradiative rate constant ($k_{nr} = (1-\Phi_{PL}) / \tau_f$).

Computational study

Computational methods:

All calculations except structure optimization at excited state were performed using Gaussian 09 package at the b3lyp/6-31g(d) level. And the structure optimization at excited state was performed at cam-b3lyp/6-311+g(d) level. The absorption and emission spectra together with the oscillator strength of SQH and SQ^- were calculated by time-dependent density functional theory (TD-DFT). Meanwhile, in SQ^- model, NH_2Et was selected as the counter-ammonium.

Table S3 Summary of the spectral data of SQH and SQ^- calculated by Gaussian 09.

		Calculation (nm)	Electronic transition	oscillator strength (f)	E_{Vert}	Experiment (nm)
Calculated absorption spectra	**SQH**	495	HOMO→LUMO (99.0%)	0.0429	$S_0 \rightarrow S_1$	310
		343	HOMO→LUMO+1 (84.5%)	0.0488	$S_0 \rightarrow S_2$	474
	SQ^-	437	HOMO→LUMO (97.8%)	0.6203	$S_0 \rightarrow S_1$	474
Calculated PL spectra	**SQH**	no emission	LUMO→HOMO (99.6%)	< 0.001	$S_1 \rightarrow S_0$	no emission
	SQ^-	465	LUMO→HOMO (95.9%)	0.6300	$S_1 \rightarrow S_0$	490

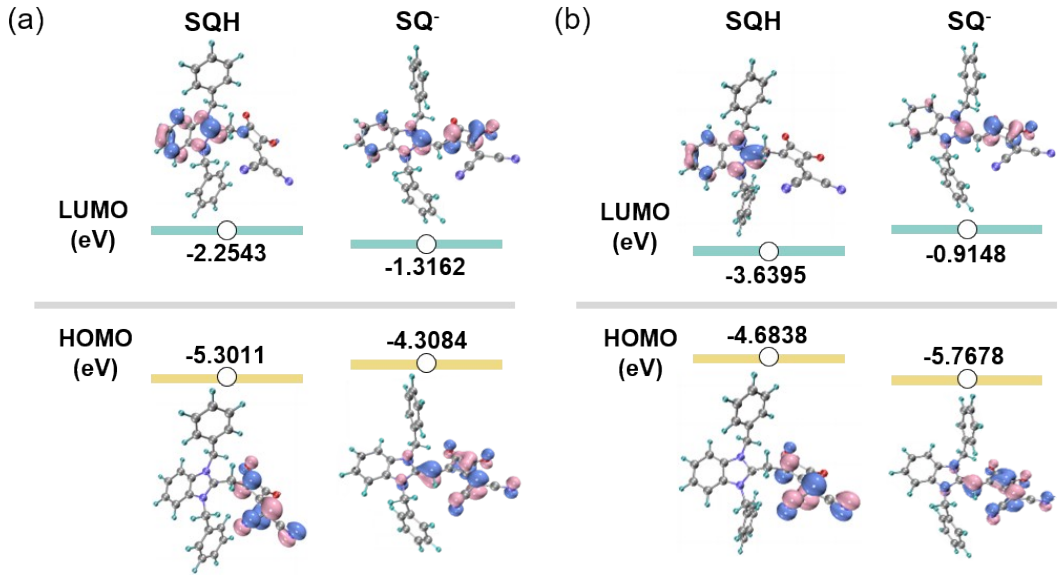

Fig. S4 (a) The theoretically calculated HOMO-LUMO gap and ground-state frontier orbitals of SQH and SQ^- by Gaussian 09; (b) The theoretically calculated HOMO-LUMO gap and excited-state frontier orbitals of SQH and SQ^- by Gaussian 09.

Preparations and characterizations of single crystals

SQH crystals were easily grown in dichloromethane/methanol eluent during the column chromatography process. With the addition of excessive ethylamine (NH_2Et), SQ-NH_3Et crystals were obtained by directly aging of SQH in dichloromethane solution. SQ-NH_2Et_2, SQ-$NHEt_3$, and SQ-NEt_4 crystals were all grown by slow diffusion of n-hexane into the dichloromethane solution containing SQH (30mg) and excessive corresponding amines (0.1 ml). To prevent weathering, SQ-NH_2Et_2 crystals were sealed in a glass tube with mother liquor for X-ray diffraction analysis. The X-ray diffraction experiments were performed with a Bruker SMART APEX-II Single-crystal diffractometer at room temperature. All structures were resolved and analyzed with the assistance of Olex2 software.

Table S4 Crystallographic data of SQH, SQ-NH_3Et, SQ-NH_2Et_2, SQ-$NHEt_3$, and SQ-NEt_4.

Sample	**SQH**	**SQ-NH_3Et**	**SQ-NH_2Et_2**	**SQ-$NHEt_3$**	**SQ-NEt_4**
CCDC number	2324687	2324688	2324689	2324690	2324691
Empirical formula	$C_{29}H_{20}N_4O_2$, 0.5(CH_2Cl_2)	$C_{29}H_{19}N_4O_2$, C_2H_8N, CH_2Cl_2	$C_{29}H_{19}N_4O_2$, $C_4H_{12}N$, 2(CH_2Cl_2)	$C_{29}H_{19}N_4O_2$, $C_6H_{16}N$	$C_{29}H_{19}N_4O_2$, $C_8H_{20}N$, CH_2Cl_2
Formula weight	448.95	586.50	699.48	557.68	670.66
T [K]	300	193(2)	296(2)	293(2)	293(2)
Crystal system	monoclinic	monoclinic	triclinic	triclinic	triclinic
Space group	P 1 21/n 1	P 21/c	P -1	P -1	P -1
a [Å]	9.0156(3)	9.8929(4)	9.914(2)	8.5686(4)	8.7961(4)
b [Å]	20.3822(6)	15.7006(7)	13.981(3)	12.3624(9)	12.3714(6)

c [Å]	14.0318(4)	19.2737(8)	15.578(3)	15.3048(10)	18.5360(8)
α [°]	90	90	63.418(5)	79.445(6)	99.727(4)
β [°]	97.518(3)	90.434(2)	72.358(6)	79.655(5)	103.102(4)
γ [°]	90	90	78.896(6)	78.006(5)	109.299(4)
V [Å^3]	2556.29(14)	2993.6(2)	1836.0(7)	1542.02(17)	1787.74(15)
Z	2	4	2	31	2
F (000)	1036	1224	728	592	708
Density [g/cm^3]	1.296	1.301	1.265	1.201	1.246
μ [mm^{-1}]	0.184	0.255	0.359	0.076	0.222
Reflections collected	28155	41888	12118	13403	20322
Unique reflections	6343	5519	6387	7053	9833
R (int)	0.023	0.063	0.050	0.030	0.027
GOF	1.055	1.050	1.065	1.032	1.053
R_1 [$I>2\sigma(I)$]	0.052	0.100	0.101	0.091	0.057
ωR_2 [$I>2\sigma(I)$]	0.122	0.277	0.274	0.250	0.117
R_1 (all data)	0.069	0.129	0.153	0.145	0.093
ωR_2 (all data)	0.132	0.300	0.311	0.292	0.137

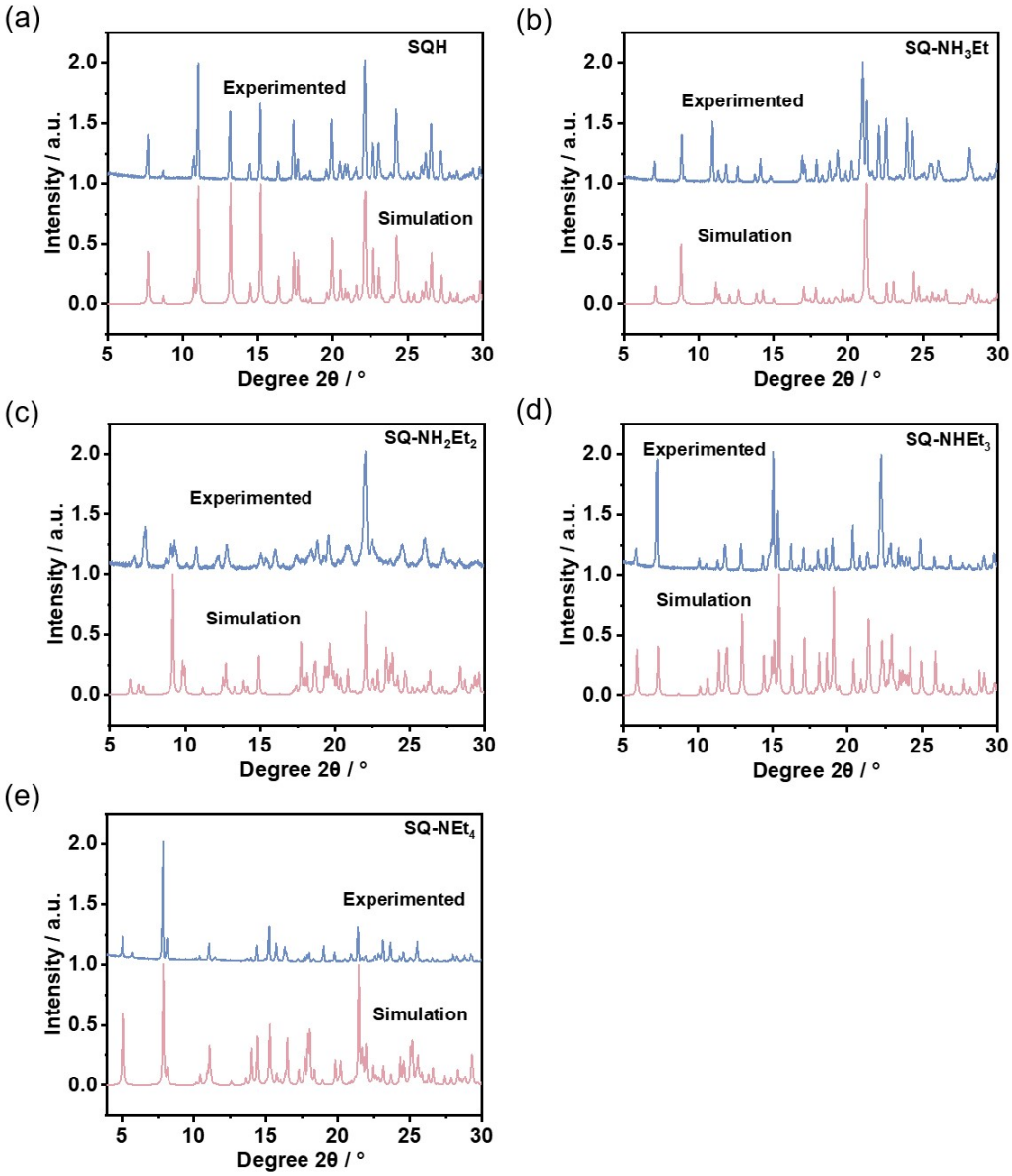

Fig. S5 PXRD patterns of (a) SQH, (b) SQ-NH_3Et, (c) SQ-NH_2Et_2, (d) SQ-$NHEt_3$, (e) SQ-NEt_4: simulated and experimented sample. (The PXRD pattern of SQ-NH_2Et_2 was acquired in a very short time after preparation of microcrystals.)

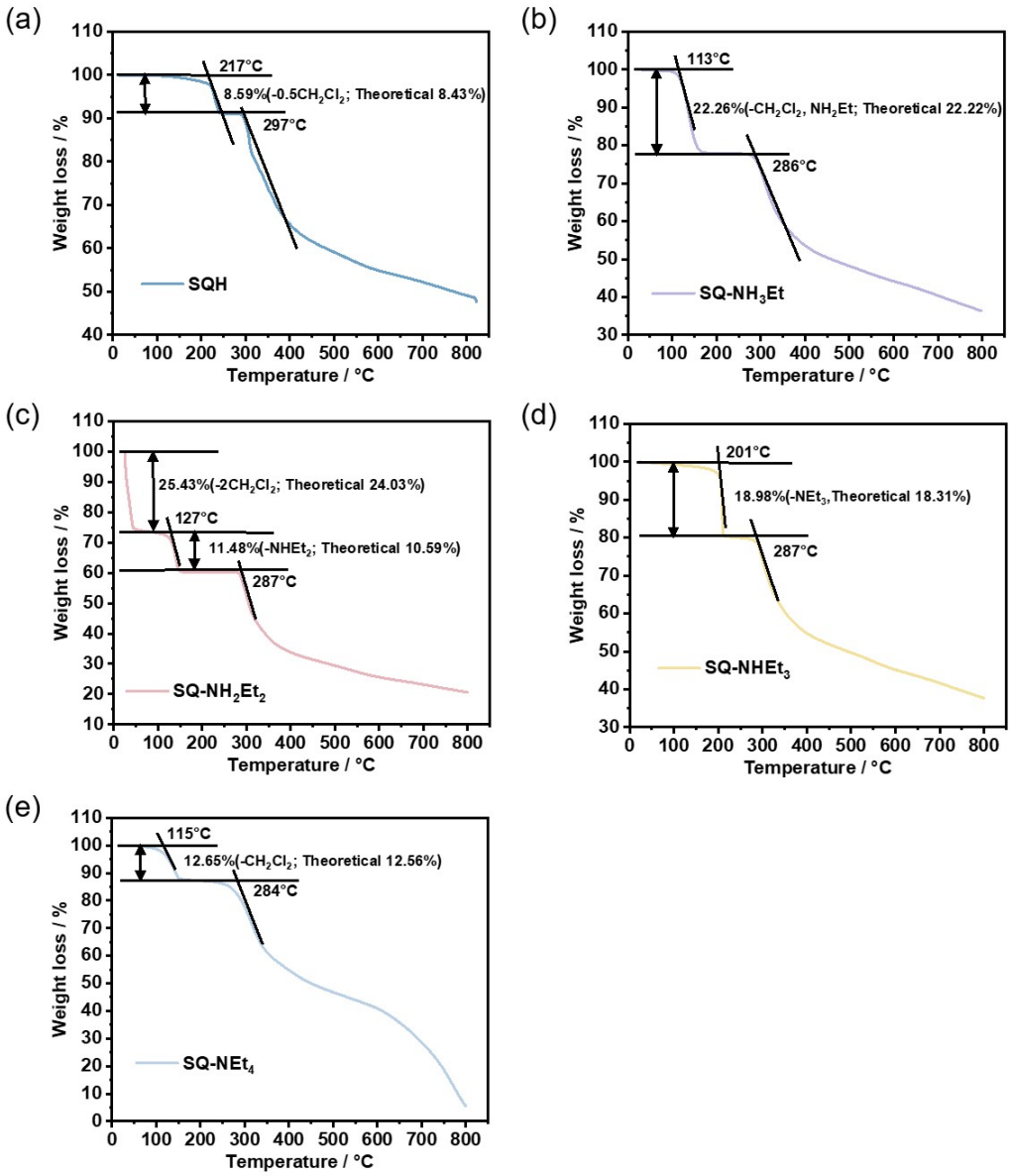

Fig. S6 TGA curves of (a) SQH, (b) SQ-NH_3Et, (c) SQ-NH_2Et_2, (d) SQ-$NHEt_3$, (e) SQ-NEt_4 microcrystals. The scanning rate is 20 °C min^{-1} under N_2.

Crystal structure analysis

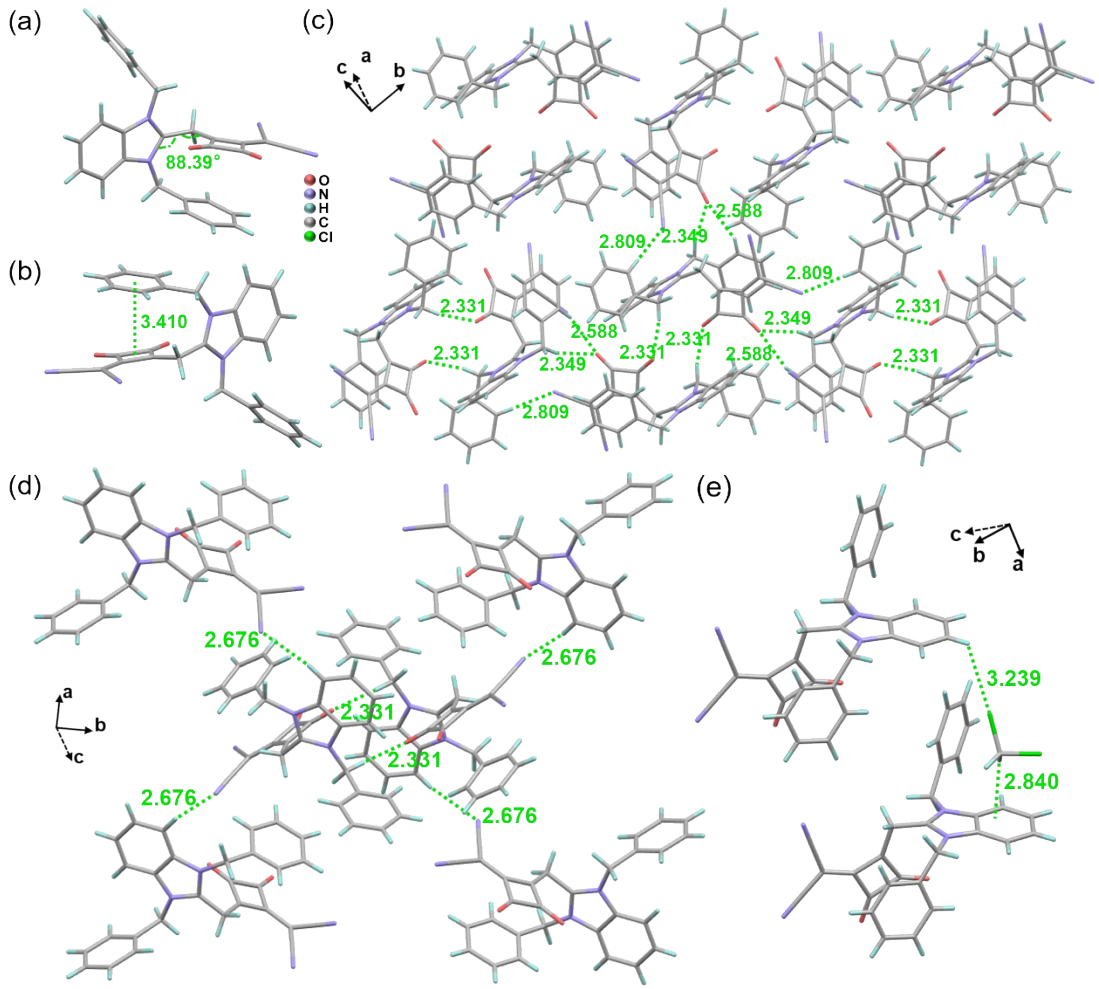

Fig. S7 The molecular structures and packing mode of the SQH crystal. (a) The dihedral angle between the cationic benzimidazole segment and anionic four-membered ring moiety. (b) intermolecular π-π interactions between benzyl segment and four-membered ring moiety. Intermolecular hydrogen-bonding interactions between adjacent SQH molecules along (c) b, c-axis, (d) a, b-axis and (e) c-axis.

SQH crystal belonged to monoclinic crystal system and crystallized in the space group of $P2_1/n$ with four SQH molecules and two CH_2Cl_2 molecules in one unit cell taking the parameters of a = 9.0156 (3) Å，b = 20.3822 (6) Å，c = 14.0318 (4) Å. In SQH molecule, the dihedral angles between the cationic benzimidazole segment and the anionic four-membered ring moiety were detected to be 88.39° (Fig. S6a), suggesting its zwitterionic feature. Two benzyl groups on the benzimidazole segment

were oriented away toward each other in SQH molecule, and intermolecular weak π-π interaction in 3.410 Å between the central four-member ring and one benzyl group was observed (Fig. S6b), which was beneficial to the formation of its exceptional zwitterionic conformation. A strong intermolecular C-H···O hydrogen bond in 2.331 Å was observed between the SQH dimers, and three types of moderate hydrogen bonds between each SQH dimer were observed in 2.588 Å (Ar-H···O), 2.676 Å (Ar-H···N) and 2.349 Å (C-H···O). Moderate Ar-H···N hydrogen bonds (2.809 Å) in adjacent SQH molecules were observed along another dimension, thus forming the final three-dimensional formations (Fig. S6c, 6d). As shown in Fig. S6e, two types of weak hydrogen bonding between CH_2Cl_2 and SQH were observed in 2.840 Å and 3.239 Å, thus stabilizing the incorporated CH_2Cl_2 solvent in SQH crystal.

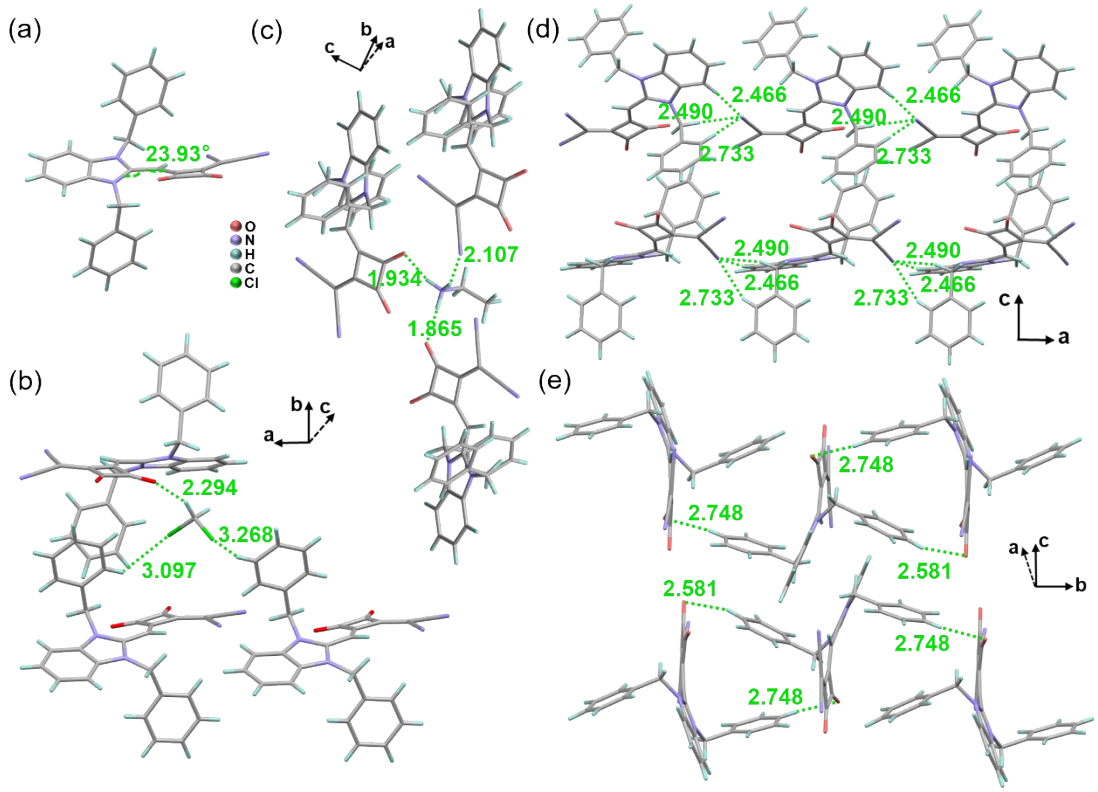

Fig. S8 The molecular structures and packing mode in the SQ-NH_3Et crystal. (a) The molecular conformation, dihedral angle between benzimidazole segment and four-membered ring moiety. (b) Intermolecular hydrogen bonds between SQ^- and CH_2Cl_2 molecule. (c) Intermolecular hydrogen bonds between counterion-ammonium and adjacent anionic SQ^- molecules. Intermolecular hydrogen-bonding interactions

between adjacent SQ^- molecules along (d) a, c-axis and (e) b-axis.

SQ-NH_3Et crystal belonged to monoclinic crystal system and crystallized in the space group of $P2_1/c$ with four SQ molecules, four $^+NH_3Et$ molecules and four CH_2Cl_2 molecules in one unit cell taking the parameters of a = 9.8929 (4) Å， b = 15.7006 (7) Å， c = 19.2737 (8) Å. In aonic SQ^- molecule the dihedral angle between benzimidazole segment and four-membered ring moiety was detected to be 23.93° (Fig. S7a), which was linked by an sp^2-hybridized carbon atom and suggested its π-conjugated feature. Similar to that in SQH crystal, two benzyl groups on the benzimidazole segment were oriented away toward each other in anion SQ^- molecule. As shown in Fig. S7b, three types of Ar(C)-H···O(Cl) hydrogen bonding between CH_2Cl_2 and SQ^- were observed in 2.294 Å, 3.097 Å and 3.268 Å, thus stabilizing the incorporated CH_2Cl_2 solvent in SQ-NH_3Et crystal. Obviously, three strong intermolecular N-H···O(N) hydrogen bonds in ~ 2.00 Å were observed between the H atom in cationic ethylamine salt and O(N) atom in anionic SQ^-, therefore ethylamine salt would be stabilized and act as a counterion for molecular packing in SQ-NH_3Et crystal (Fig. S7c). Moreover, multiple intermolecular Ar(C)-H···O(N) hydrogen bonds in the region between 2.466 and 2.748 Å were observed in adjacent SQ^- molecules, thus forming the final three-dimensional formations (Fig. S7d).

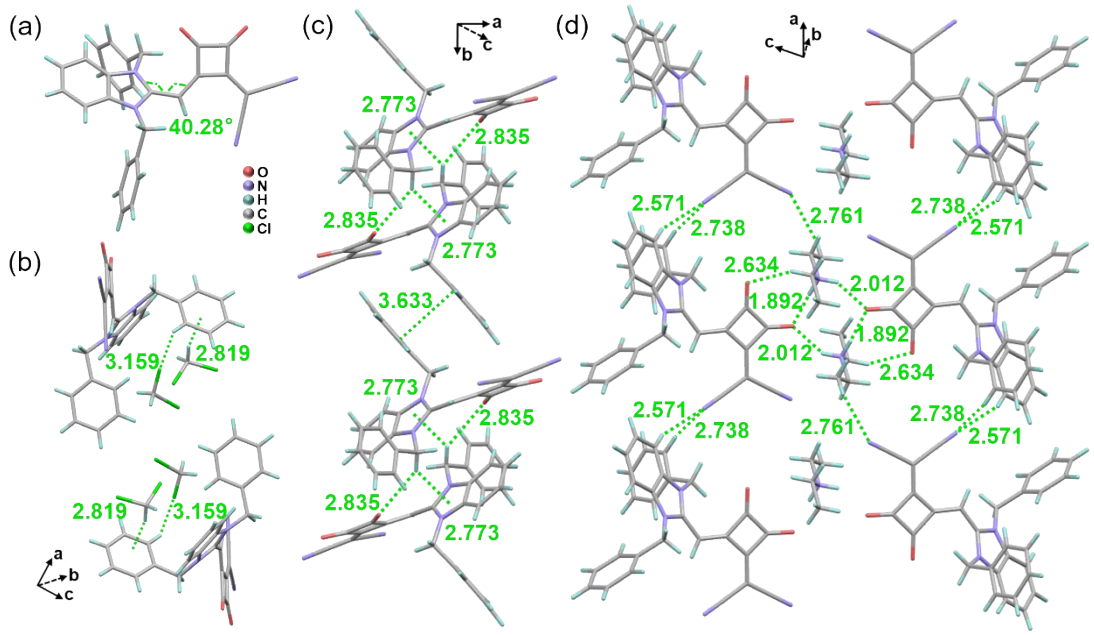

Fig. S9 The molecular structures and packing mode in the SQ-NH_2Et_2 crystal. (a) The molecular conformation, dihedral angle between benzimidazole segment and four-membered ring moiety. (b) Intermolecular hydrogen bonds between SQ^- and CH_2Cl_2 molecule. (c) Intermolecular π-π interactions between phenyl segment in adjacent SQ^- molecules and intermolecular hydrogen-bonding interactions between adjacent SQ^- molecules along a, b-axis. (d) Intermolecular hydrogen bonds between diethylamine salt and adjacent SQ^- molecules, together with intermolecular hydrogen-bonding interactions between adjacent SQ^- molecules along a, c-axis.

SQ-NH_2Et_2 crystal belonged to triclinic crystal system and crystallized in the space group of P-1 with two SQ^- molecules, two $^+NH_2Et_2$ molecules and four CH_2Cl_2 molecules in one unit cell taking the parameters of a = 9.914 (2) Å， b = 13.981 (3) Å， c = 15.578 (3) Å. In aonic SQ^- molecule the dihedral angles between benzimidazole segment and four-membered ring moiety were detected to be 40.28° (Fig. S8a), which was also linked by an sp^2-hybridized carbon atom and suggested its π-conjugated feature. Two benzyl groups on the benzimidazole segment were oriented toward each other in anion SQ^- molecule. It is worth mentioning that very weak hydrogen bonds in 2.819 Å and 3.159 Å can be observed between CH_2Cl_2 molecules and adjacent SQ^- molecules along a, c-axis, which means that the CH_2Cl_2 solvent is easy to escape from

the SQ-NH_2Et_2 crystal and responds to the observed vapoluminescence behavior of SQ-NH_2Et_2 crystal at room temperature (Fig. S8b). Intermolecular weak π-π interactions in 3.633 Å between phenyl segments in adjacent SQ^- molecules were observed, thus forming a dimeric unit and benefiting the crystal emission. Meanwhile, intermolecular C-H···O(π) hydrogen bonds in 2.835 Å and 2.773 Å were observed in each adjacent dimeric unit (Fig. S8c). Other two intermolecular Ar-H···N hydrogen bonds in 2.571 and 2.738 Å were observed in adjacent SQ^- molecules, thus forming the final three-dimensional fomations. Along a, c-axis, two types of strong intermolecular N-H···O hydrogen bonds in 1.892 Å and 2.012 Å were observed between the H atom in cationic diethylamine salt and O atom in anionic SQ^-, together with two weak C-H···O hydrogen bonds in 2.634 Å and 2.761 Å, therefore diethylamine salt would be stabilized and act as a counterion for molecular packing in SQ-NH_2Et_2 crystal (Fig. S8d).

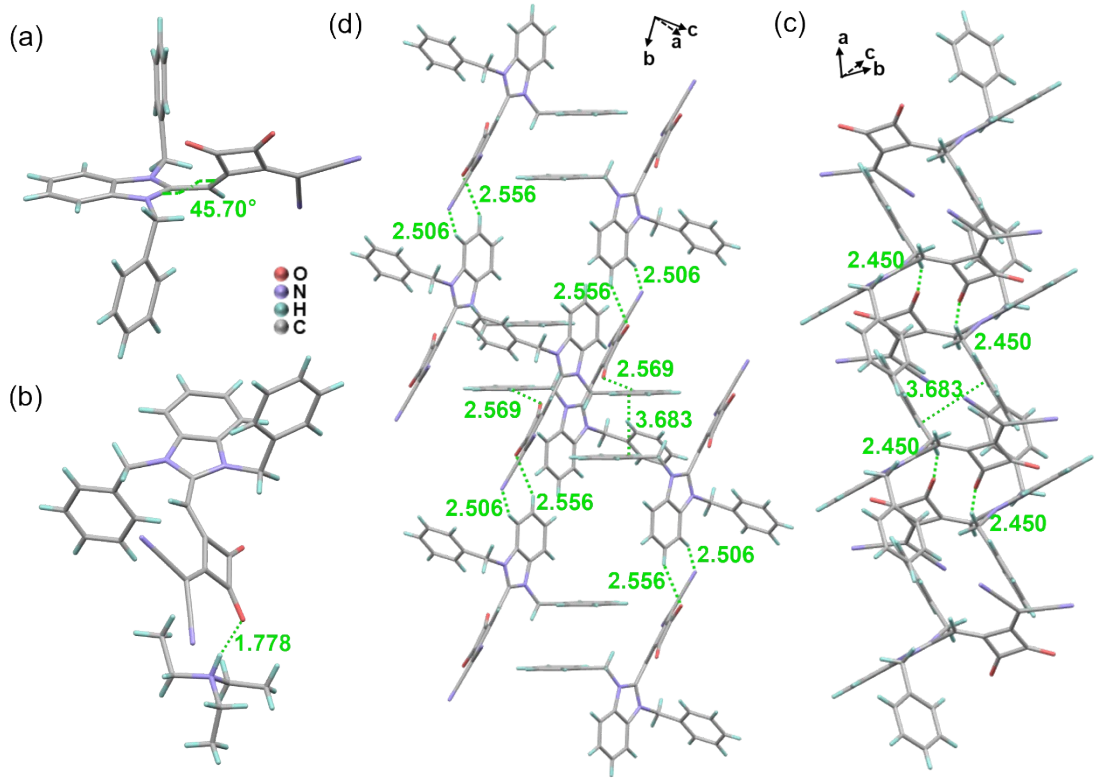

Fig. S10 The molecular structures and packing mode in the SQ-$NHEt_3$ crystal. (a) The molecular conformation, dihedral angles between benzimidazole segment and four-membered ring moiety. (b) Intermolecular hydrogen bonds between counterion-ammonium and adjacent anionic SQ^- molecules. (c) Intermolecular π-π interactions

between phenyl segment in adjacent SQ^- molecules and intermolecular hydrogen-bonding interactions between adjacent SQ^- molecules along b, c-axis. (d) Intermolecular hydrogen bonds between adjacent SQ^- molecules along a, b-axis.

$SQ\text{-}NHEt_3$ crystal belonged to triclinic crystal system and crystallized in the space group of P-1 with two SQ^- molecules and two $^+NHEt_3$ molecules in one unit cell taking the parameters of a = 8.5686 (4) Å， b = 12.3624 (9) Å， c = 15.3028 (10) Å. In anionic SQ^- molecule, the dihedral angle between the benzimidazole segment and the four-membered ring moiety was detected to be 45.70° (Fig. S9a), which was also linked by a sp^2-hybridized carbon atom and suggested its π-conjugated feature. A strong intermolecular N-H···O hydrogen bond in 1.778 Å was observed between the H atom in cationic triethylamine salt and the O atom in anionic SQ^-, therefore triethylamine salt would be stabilized and act as a counterion for molecular packing in $SQ\text{-}NHEt_3$ crystal (Fig. S9b). Intermolecular Ar-H···O hydrogen bonds in 2.569 Å were observed between adjacent SQ^- molecules, thus forming a dimeric unit. Meanwhile, two benzyl groups on the benzimidazole segment were oriented toward each other in anion SQ^- molecule, and intermolecular weak π-π interactions in 3.683 Å between adjacent phenyl segments in a dimeric unit, which benefits the crystal emission (Fig. S9c). What's more, multiple intermolecular Ar(C)-H···O(N) hydrogen bonds in the region between 2.450 and 2.556 Å were observed in adjacent SQ^- molecules, thus forming the final three-dimensional formations (Fig. S9c, 9d).

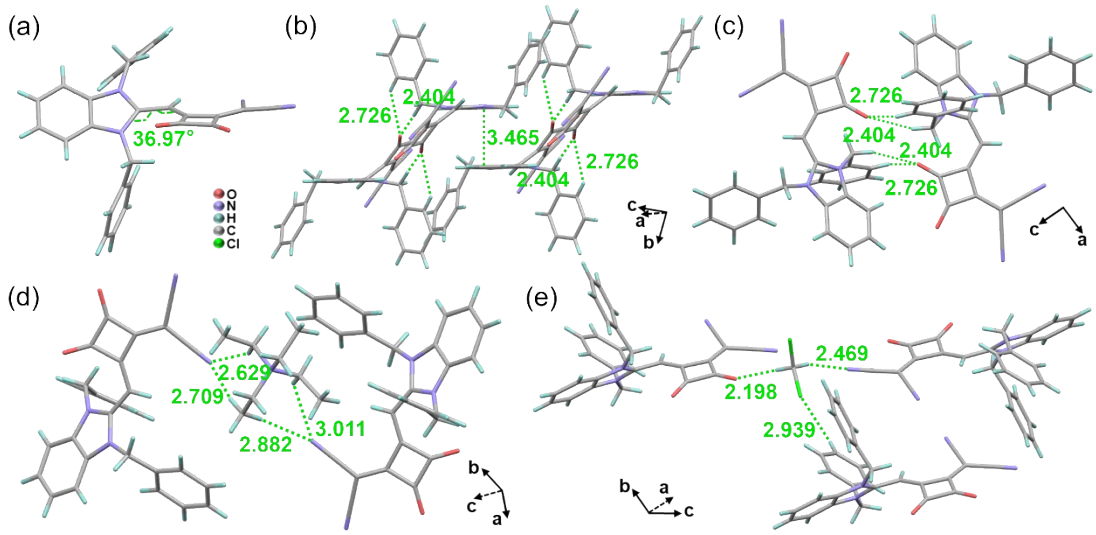

Fig. S11 The molecular structures and packing mode in the SQ-NEt_4 crystal. a) The molecular conformation, dihedral angle between benzimidazole segment and four-membered ring moiety. b) Intermolecular π-π interactions between benzimidazole segment in adjacent SQ^- molecules. c) Intermolecular C-H···O hydrogen bonds between phenyl segment and four-membered ring moiety in adjacent SQ^- molecules. d) Intermolecular hydrogen bonds between counterion-ammonium and adjacent anionic SQ^- molecules. e) Multiple intermolecular hydrogen bonds between CH_2Cl_2 and adjacent SQ^- molecules.

SQ-NEt_4 crystal belonged to triclinic crystal system and crystallized in the space group of P-1 with two SQ^- molecules, two $^+NEt_4$ molecules and two CH_2Cl_2 molecules in one unit cell taking the parameters of a = 8.7961 (4) Å，b = 12.3714 (6) Å，c = 18.5360 (8) Å. In aonic SQ^- molecule the dihedral angle between benzimidazole segment and four-membered ring moiety was detected to be 36.97° (Fig. S10a), which was also linked by a sp^2-hybridized carbon atom and suggested its π-conjugated feature. Two benzyl groups on the benzimidazole segment were oriented toward each other in anion SQ^- molecule. Intermolecular C-H···O hydrogen bonds in 2.404 Å and 2.726 Å were observed between adjacent SQ molecules, thus forming a dimeric unit. And intermolecular weak π-π interactions in 3.465 Å between adjacent benzimidazole segments in a dimeric unit, which would quench the crystal emission (Fig. S10b, 10c).

Multiple intermolecular hydrogen bonds in the region of 2.629 Å and 3.011 Å were observed between the H atom in cationic tetraethylamine salt and N atom in anionic SQ^-, therefore tetraethylamine salt would be stabilized and act as a counterion for molecular packing in SQ-NEt_4 crystal (Fig. S10d). Different from that in SQ-NH_2Et_2 crystal, three types of moderate hydrogen bonds in the region of 2.198 Å and 2.939 Å can be observed between CH_2Cl_2 molecules and adjacent SQ^- molecules, thus ensuring the stabilization of incorporated CH_2Cl_2 solvents (Fig. S10e).

Characterizations of vapoluminescence behavior

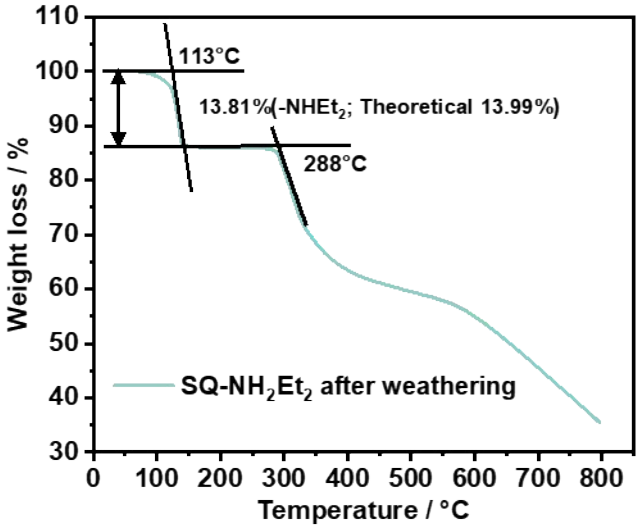

Fig. S12 TGA curves of SQ-NH_2Et_2 microcrystals after weathering. The scanning rate is 20 °C min^{-1} under N_2.

^{1}H NMR, ^{13}C NMR and MS spectra

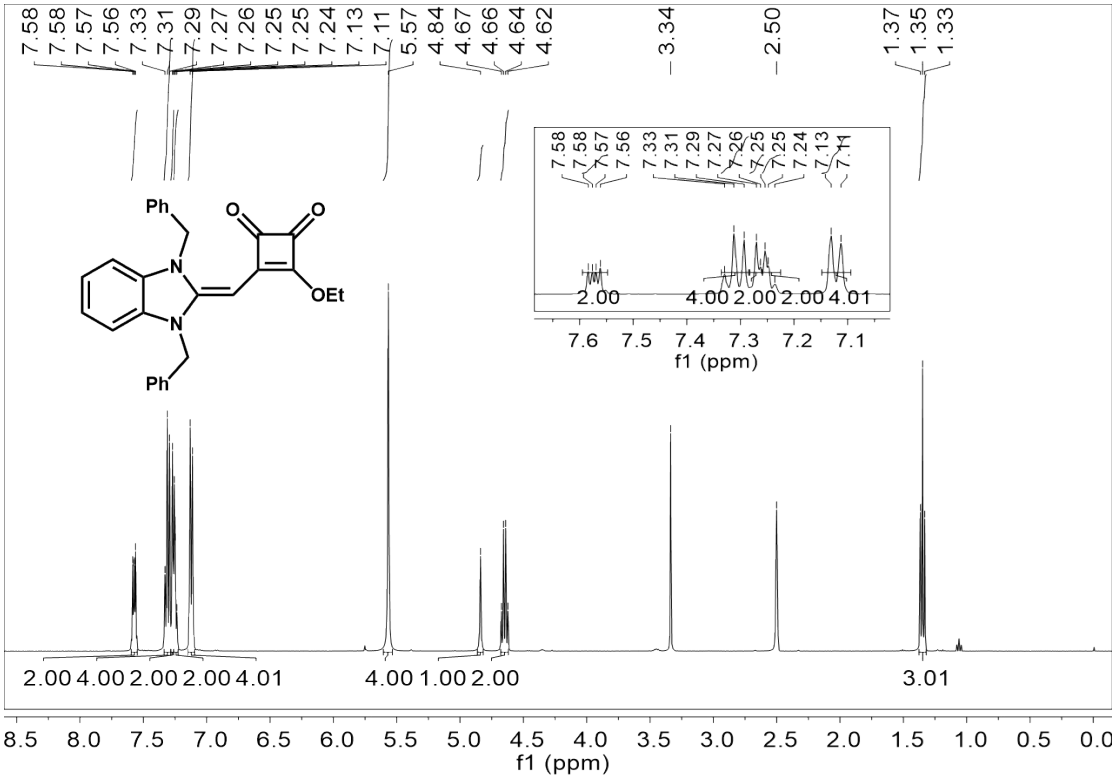

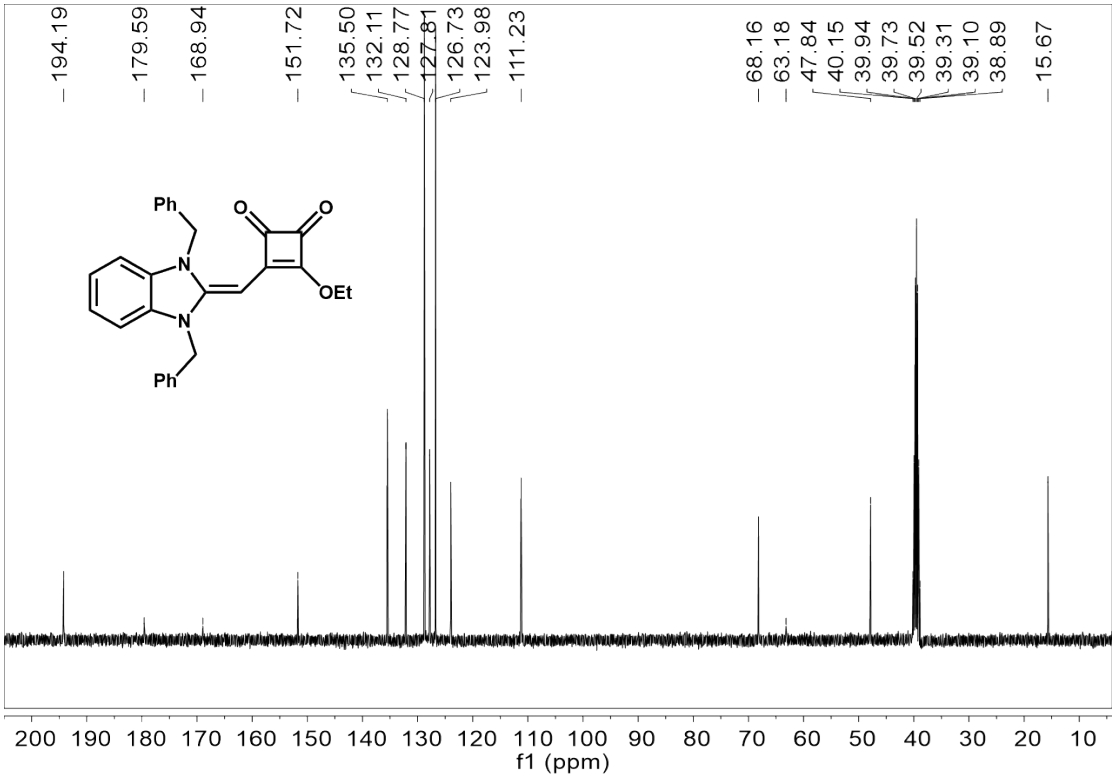

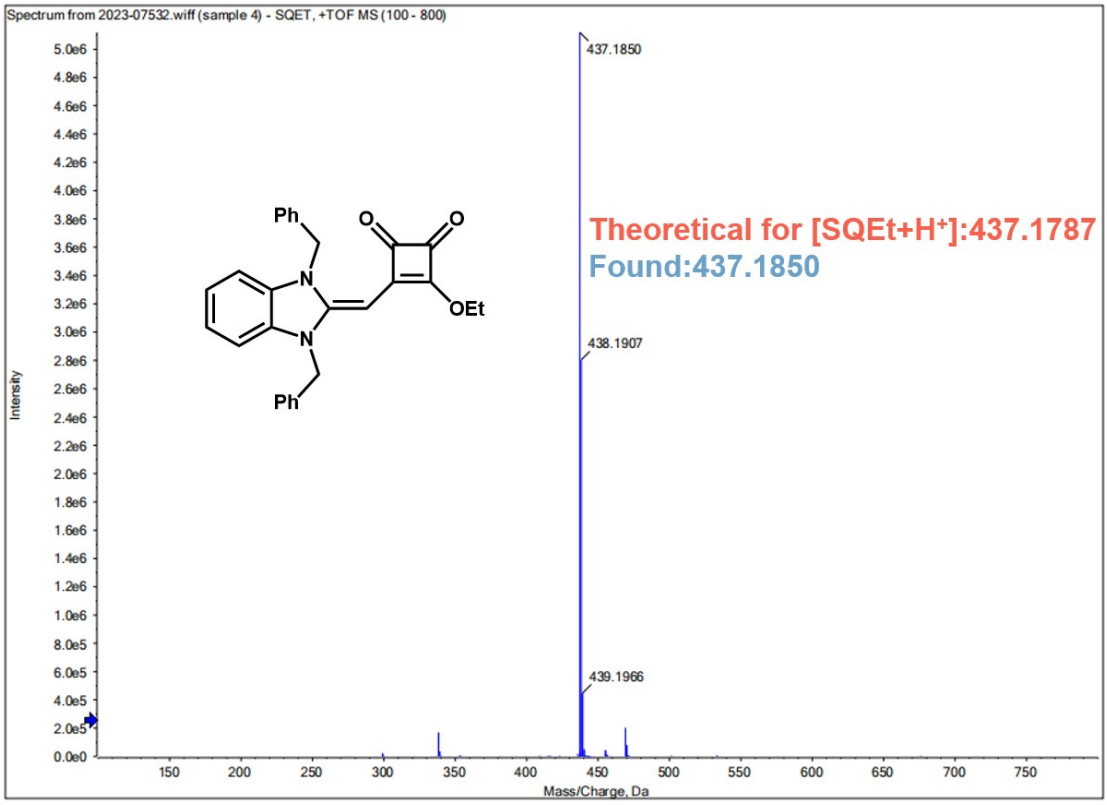
Spectrum from 2023-07532.wiff (sample 4) - SQET, +TOF MS (100 - 800)
Intensity
Mass/Charge, Da
437.1850
438.1907
439.1966
Ph
O
O
OEt
N
N
Ph
Theoretical for [SQEt+H+]:437.1787
Found:437.1850

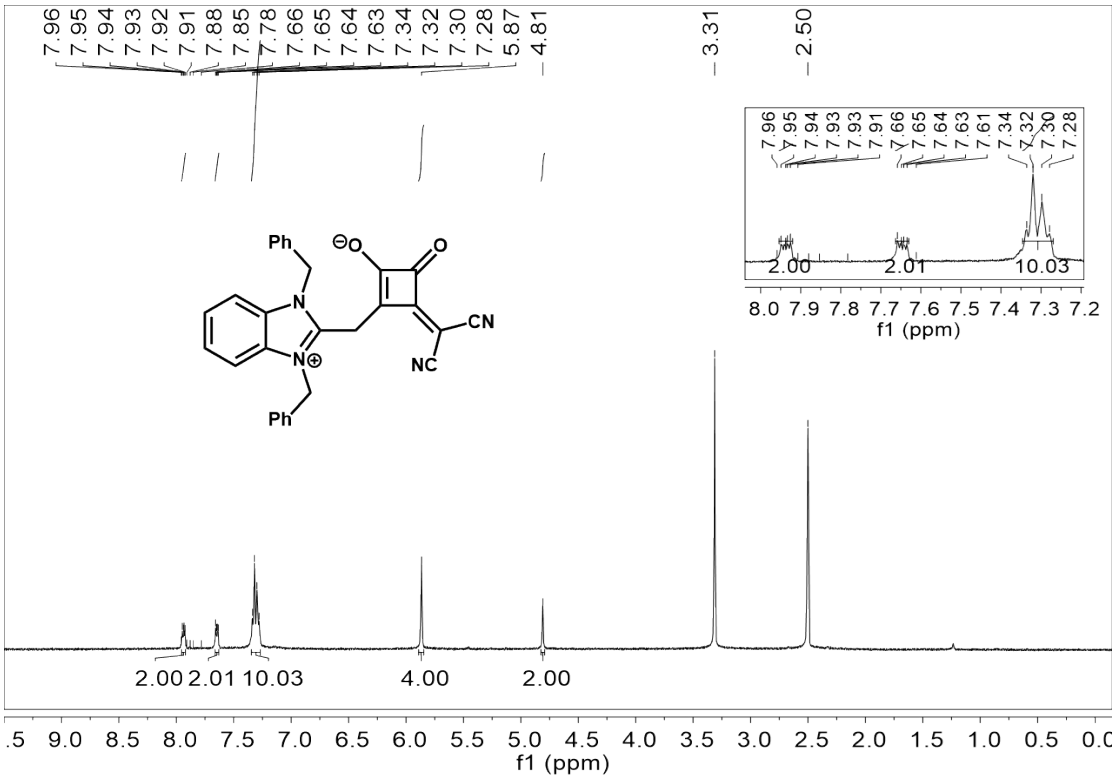
7.96 7.95 7.94 7.93 7.92 7.91 7.88 7.85 7.78 7.66 7.65 7.64 7.63 7.34 7.32 7.30 7.28 5.87 4.81 3.31 2.50
Ph
⊖O
O
N
N⊕
Ph
CN
NC
2.00 2.01 10.03
4.00
2.00
f1 (ppm)

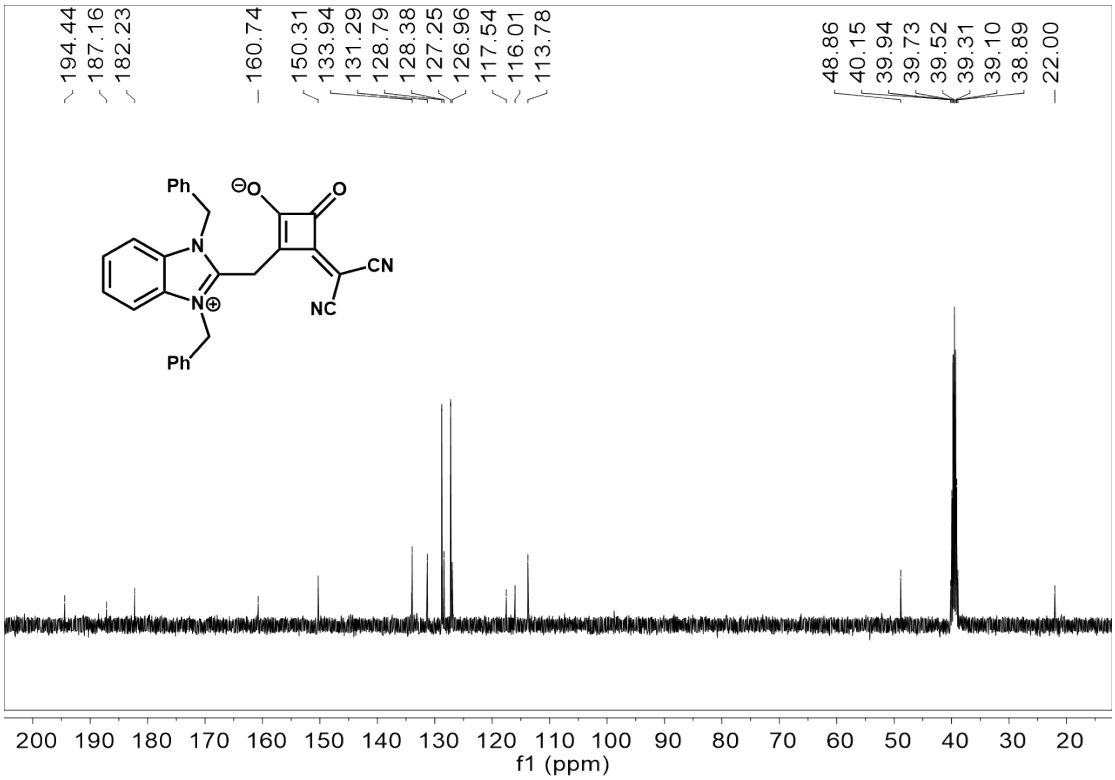
194.44
187.16
182.23
160.74
150.31
133.94
131.29
128.79
128.38
127.25
126.96
117.54
116.01
113.78
48.86
40.15
39.94
39.73
39.52
39.31
39.10
38.89
22.00
Ph
O
O
N
CN
NC
N
Ph
200 190 180 170 160 150 140 130 120 110 100 90 80 70 60 50 40 30 20
f1 (ppm)

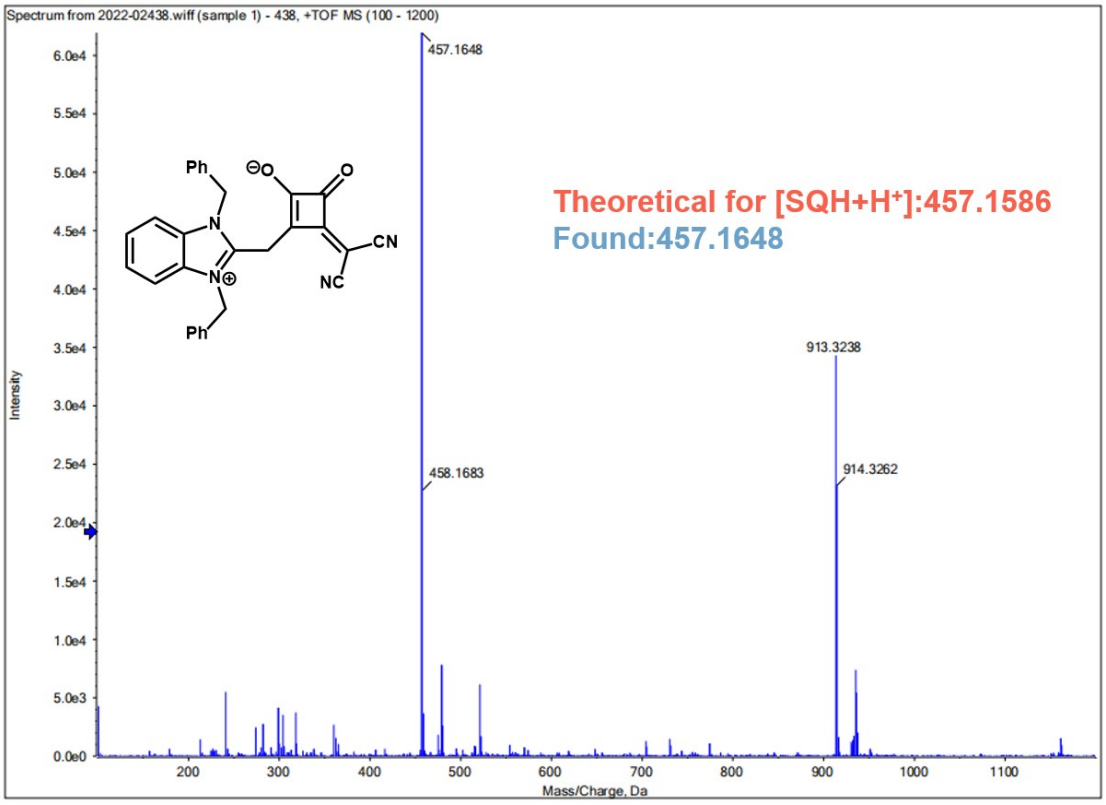
Spectrum from 2022-02438.wiff (sample 1) - 438, +TOF MS (100 - 1200)
457.1648
458.1683
913.3238
914.3262
Theoretical for [SQH+H+]:457.1586
Found:457.1648
Intensity
6.0e4
5.5e4
5.0e4
4.5e4
4.0e4
3.5e4
3.0e4
2.5e4
2.0e4
1.5e4
1.0e4
5.0e3
0.0e0
200
300
400
500
600
700
800
900
1000
1100
Mass/Charge, Da

Reference

1 G. Xia, Z. Wu, Y. Yuan, H. Wang, The regioselectivity and synthetic mechanism of 1,2-benzimidazolesquaraines: combined experimental and theoretical studies, *RSC Adv.*, 2013, **3**, 18055 –18061.